electronics

MDPI

Article

Demodulating Optical Wireless Communication of FBG Sensing with Turbulence-Caused Noise by Stacked Denoising Autoencoders and the Deep Belief Network

Shegaw Demessie Bogale †, Cheng-Kai Yao †, Yibeltal Chanie Manie, Amare Mulatie Dehnaw, Minyechil Alehegn Tefera, Wei-Long Li, Zi-Gui Zhong and Peng-Chun Peng *

Department of Electro-Optical Engineering, National Taipei University of Technology, Taipei 10608, Taiwan; t112659403@ntut.edu.tw (S.D.B.); t109658093@ntut.org.tw (C.-K.Y.); yibeshmamaru@gmail.com (Y.C.M.); mulatieamare7@gmail.com (A.M.D.); t110659401@ntut.org.tw (M.A.T.); t112658007@ntut.org.tw (W.-L.L.); t112658080@ntut.org.tw (Z.-G.Z.)

* Correspondence: pcpeng@ntut.edu.tw; Tel.: +886-2-2771-2171 (ext. 4671)

† These authors contributed equally to this work.

Abstract: Free-space optics communication (FSO) can be used as a transmission medium for fiber optic sensing signals to make fiber optic sensing easier to implement; however, interference with the sensing signals caused by the optical turbulence and scattering of airborne particles in the FSO path is a potential problem. This work aims to deep denoise sensed signals from fiber Bragg grating (FBG) sensors based on FSO link transmission using advanced denoising deep learning techniques, such as stacked denoising autoencoders (SDAE). Furthermore, it will demodulate the sensed wavelength of FBGs by applying the deep belief network (DBN) technique. This is the first time the real FBG sensing experiment has utilized the actual noise interference caused by the environmental turbulence from an FSO link rather than adding noise through numerical processing. Consequently, the spectrum of the FBG sensors is clearly modulated by the noise and the issue with peak power variation. This complicates the determination of the center wavelengths of multiple stacked FBG spectra, requiring the use of machine learning techniques to predict these wavelengths. The results indicate that SDAE is efficient in denoising from the FBG spectrum, and DBN is effective in demodulating the central wavelength of the overlapped FBG spectrum. Thus, it is beneficial to implement an FSO link-based FBG sensing system in adverse weather conditions or atmospheric turbulence.

Keywords: free-space optics communication; fiber Bragg grating; signal denoising; machine learning; peak-wavelength prediction

Citation: Bogale, S.D.; Yao, C.-K.; Manie, Y.C.; Dehnaw, A.M.; Tefera, M.A.; Li, W.-L.; Zhong, Z.-G.; Peng, P.-C. Demodulating Optical Wireless Communication of FBG Sensing with Turbulence-Caused Noise by Stacked Denoising Autoencoders and the Deep Belief Network. *Electronics* **2024**, *13*, 4127. https://doi.org/10.3390/electronics13204127

Academic Editors: Wenyu Zhang, Tianwei Hou and Sherali Zeadally

Received: 15 September 2024
Revised: 16 October 2024
Accepted: 18 October 2024
Published: 20 October 2024

1. Introduction

In situations requiring accurate measurements of strain [1], temperature [2], water level [3], pressure [4], chemistry [5], manufacture [6], and vibration [7], FBG sensors have emerged as a highly useful instrument in these relevant applications. Combining FBG sensors with FSOs enables long-distance transmission without needing physical fiber optic connections, circumventing cable laying and terrain obstacles. Consequently, this integration approach's flexibility, deployment speed, and cost-effectiveness are all very favorable [8,9]. However, in real-world applications, FSOs might introduce extra spectral noise because of ambient turbulence in addition to the spectral noise issue brought on by fiber damage in FBGs [10–12]. All these aggravate the difficulty of FBG sensing. Many papers have investigated the problem of noise interference in FBG spectra, in which noise reduction, de-noising, and machine learning are utilized to interrogate the FBG spectra to obtain sensing information to solve the noise interference problem [13–18]. However, the noise interference of FBG sensing based on FSO architecture has never been studied.

Incidentally, while distributed fiber optic sensing systems can integrate FSOs, they have not yet explored the potential noise effects of these integrations [19].

To enhance the capacity of the FBG sensor arrangement and improve sensing efficiency, it is crucial to address the spectral overlap issue arising from using multiple FBGs. The overlapping spectra of FBGs present challenges in identifying the center wavelength of the FBGs for interpreting sensed information. This challenge can be effectively mitigated through the application of machine learning techniques. The challenge of spectral overlap in FBG and the issue of demodulating spectral incidental noise have been documented in the existing literature. For instance, previous studies have successfully addressed these challenges using methods such as integrating discrete wavelet transform denoising and long short-term memory [13], employing a convolutional neural network-based autoencoder [14], integrating a convolutional time-domain audio separation network and long short-term memory [16], and utilizing a convolutional time-domain audio separation network [18]. These approaches have demonstrated the ability to demodulate the FBG overlapping spectrum in the presence of noise.

In the transmission channel of FSO, the airflow can alter the air density and refractive index [20], and it may contain various airborne particles. Consequently, in cases of high air pollution and strong airflow, the transmission power of the FSO may fluctuate over time. Photons emitted by the FSO will encounter airborne particles, leading to scattering. Additionally, rapid changes in refractive index can cause optical turbulence, resulting in scintillation from beam distortion, which can seriously interfere with the FBG spectra by creating noise. Previous studies have shown that machine learning such as DBN, with its strong interpretation capability, can effectively solve the FBG overlapping problem [21]. However, it remains to be verified whether DBN can still effectively solve the wavelength interpretation of FBG spectra under overlapping conditions to successfully interrogate the sensed information when subjected to the noise additions caused by FSO devices. According to the above question, it is conceivable to use DBN to interpret the FBG spectrum with and without FSO noise, and the FBG spectrum without noise will surely enable DBN to obtain better results in wavelength interrogation. Previous research results have demonstrated that when using machine learning to interpret signals, the denoised signals can be more accurately interpreted by machine learning [22]. This is because noise blurs the signal characteristics, which may result in the loss of key information, and the chaotic effect of noise may cause the same signal to be recognized as a different signal. To this end, it is necessary to perform denoising before wavelength demodulation using machine learning to obtain better-interrogated results for FBG spectra experiencing FSO noise. SDAE is an unsupervised neural network model for feature extraction and dimensionality reduction in deep learning and works by stacking multiple denoising autoencoders. This model has a wide range of applications in many fields, such as image processing, natural language processing, and machine translation [23–25]. Therefore, SDEA will serve to clean the FBG spectrum from the noise traces due to the interference from FSO noise, thus converting the FBG spectrum into a smooth curve for subsequent demodulation of the sensed wavelengths of the FBGs using machine learning.

This paper proposes an integrated machine learning system to demodulate sensed information in the presence of FBG spectral noise due to optical turbulence and particle scattering in the FSO channel, first utilizing SDAE for noise reduction and DBN to detect the peak wavelengths of each FBG sensor in both overlapping and non-overlapping spectra. To discern between noise and correlation, SDAE applies a deep learning technique to learn the underlying structure of the clean sensor signals. The FBG spectrum is denoised by SDAE to improve signal clarity, which enables the DBN to interpret sensor readings more accurately. Hence, for resolving noise and peak detection issues, this combined approach improves the accuracy and dependability of FBG sensor data and is especially well-suited for sensing environments where ambient turbulence contributes to noise in FSO transmissions.

Key novelties of the work and heavyweight clarifications:

- The proposed work integrates the SDAE and DBN models to demodulate the FBGs overlapping sensing spectra of FSO transmission with incidental noise due to optical turbulence and scattering.
- In addition to the spectrum being inlaid with noise, the peak power of individual FBGs after denoising is different even if the wavelength position of individual FBGs is set in the same situation. That is, the wavelengths of the FBGs under the same conditions can be demodulated by DBN even if the peak power of the FBGs is different each time the data are collected.
- In the past, the utilization of demodulation based on FBG spectral denoising lacked strong practical relevance and applicability. This was primarily due to optical fibers being usually well-protected and not easily damaged. Significantly induced noise in the spectrum required a substantial optical loss of 25 dB or more, as it emits a beam power of 10 dB. Even if the fiber is severely damaged, the optical switch could be employed to reroute the fiber transmission path, obviating the necessity for denoising in purely fiber optic systems. Conversely, the application relevance and applicability of denoising in systems with FSO communication are substantial.
- The length of the FSO link is not the focus of this paper, and an increase in the length of the FSO link usually only increases optical loss. This work aims to investigate the demodulation of FBG spectra by the noise generated by ambient turbulence in the FSO path. In addition, according to the systematic tests in this work, the pouring of water and fog into the FSO path only produces optical loss and does not impose noise on the spectrum. Even in the case of heavy rain, there is a possibility that the FBG spectrum may be impaired. However, the spectrum with noise has already been collected from the FSO transmission that is disturbed by the airflow, so there is no need to collect data specifically from rainy days. In addition, weather conditions are difficult to control.

2. Experimental Setup

The experimental setup is shown in Figure 1. The broadband light source (BLS) first emits a probe beam, which is routed to the 2 m FSO link by port 1 of the circulator (Cir.) to port 2 of the circulator for transition and then transmitted to the FBG array. The sensing information, sensed by the FBG array and its reflected Bragg wavelength, will be returned originally, first through the FSO link and then by port 2 of the circulator to port 3 of the circulator, and then to the optical spectrum analyzer for sensing spectral presentation. The collected spectrum is finally transmitted to the PC for machine-learning AI for denoising and FBG wavelength demodulation. The initial three FBG wavelengths are separated as shown in the upper right corner of Figure 1. The wavelength variation of the FBG sensing spectrum is realized by applying strain to the FBG sensor.

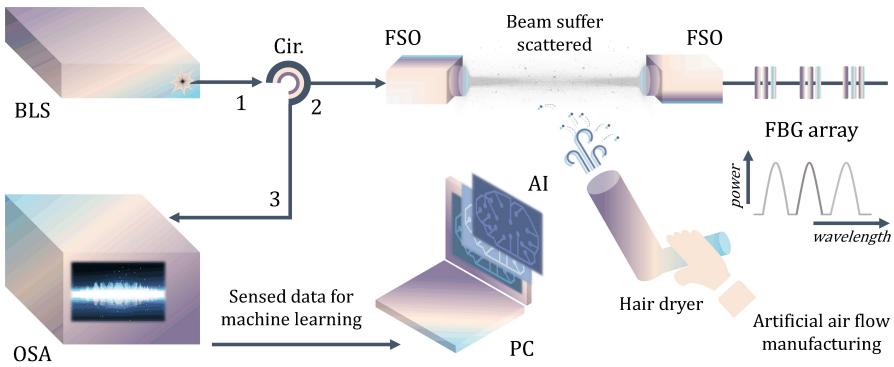

Figure 1. Experimental framework for FBG array sensing based on FSO transmission with incidental particle scattering. The sensed data are used for AI model training and testing. (BLS: broadband light source; Cir.: circulator; OSA: optical spectrum analyzer; PC: personal computer).

In addition, to create ambient turbulence in the FSO channel, a strong airflow is manually ejected through the FSO transmission path by a hair dryer. The presence of air currents induces fluctuations in air density within the FSO transmission channel, leading to variations in the refractive index over time. This phenomenon gives rise to optical turbulence and consequent scintillation, causing variations in power and incidental noise in the FBG spectrum. The scintillation index ${\sigma_1}^2$ can be expressed as Formula (1) [26]:

$$ {\sigma_1}^2 = 1.23 \cdot {C_n}^2 \cdot K^{\frac{7}{6}} \cdot L^{\frac{11}{6}} \quad (1) $$

where ${C_n}^2$ is the refractive index structural parameter, K is the wave number, and L is the transmission distance. Moreover, the airflow will attach a large number of air particles and will accelerate the particles through the FSO transmission path, which increases the probability of the beam contacting with the air particles in the relative period and causes scattering. As a result, the scattering causes some wavelengths of the beam to deviate from their original trajectories, which also results in noise embedded in the FBG spectrum, and the noise pattern changes with time. The wind speeds generated by the hair dryer used in the experiment were in the range of 2.5 m/s to 3.1 m/s, and the fluctuations were usually 0.2 m/s. To obtain the turbulence intensity (TI), Formula (2) is generally used as follows:

$$ TI = (\sigma_2 / V) \times 100 \quad (2) $$

where σ_2 is the standard deviation of wind speed (m/s) and V is the mean wind speed (m/s). Therefore, it is estimated that the turbulence intensity generated by the experimental setup is between 3% and 10%, which is in the range of medium and high turbulence. The proposed SDAE and DBN model was implemented using the TensorFlow 2. 10. 0 framework, along with the Keras and Sklearn libraries. The training was conducted on a PC equipped with an Intel Core i7-4790 3.60 GHz CPU and 20 GB of RAM.

3. Data Collection and SDAE Denoise

In the data collection section, three FBGs were used, in which the reflected wavelength of FBG 1 was defined as changing, and the reflected wavelengths of FBG 2 and FBG 3 were fixed at 1546.3 nm and 1546.69 nm, respectively. The reflected wavelength of FBG 1 underwent 16 strain steps from the beginning of the change to the end of the change, and the corresponding wavelengths were 1545.95 nm, 1546.01 nm, 1546.07 nm, 1546.13 nm, 1546.19 nm, 1546.25 nm, 1546.36 nm, 1546.44 nm, 1546.52 nm, 1546.6 nm, 1546.68 nm, 1546.76 nm, 1546.84 nm, 1546.92 nm, 1547 nm, and 1547.08 nm, respectively, as presented in Figure 2. In addition, the wavelength difference of FBG 1 is 0.06 nm for each step before the 7th strain step, while the wavelength difference of FBG 1 is 0.08 nm for each step after the 7th strain step; this inconsistency is to verify the performance of the wavelength demodulation function of machine learning. It is also used to misalign the wavelengths of FBG 1 and FBG 2 since there is no need for demodulation when the wavelengths are the same. The total number of spectra collected is 304, namely, 19 spectra with different noise patterns are collected for each strain step.

SDAE is a neural network designed to reconstruct clean data from noisy observations, and its architecture consists of multiple layers of autoencoders stacked on top of each other. Each autoencoder learns to encode and decode the input data through its hidden layer. The layered structure of SDAE allows it to capture and reconstruct the fine details of a clean FBG spectrum, even when the FBG spectrum has significant noise problems. Prior to the application of SDAE, each of the collected data contained wavelength and intensity values representative of the original sensor data, which were subjected to an initial cleaning process to deal with missing values and anomalies. Subsequently, data standardization is performed to normalize the input features to ensure that the scaling of the input SDAE and DBN models is consistent. Common normalization methods include min–max scaling, which rescales the intensity values to a range between 0 and 1. After data processing, the dataset is divided into a training set (80%) and a test set (20%). The coding process isolates

the relevant noise signal features, while the decoding process reconstructs the noise-cleared spectrum to produce less distorted and more accurate data for further analysis. Thus, the final layered structure of the SDAE ensures that the main features of the FBG spectrum are preserved and the noise is effectively suppressed.

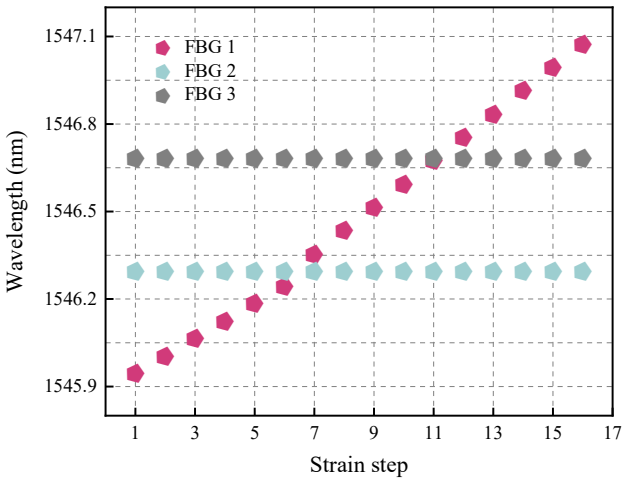

Figure 2. The corresponding values of the three FBG reflected wavelengths in each strain step.

Figure 3a shows the cross-contrast of some spectra before and after denoising with SDAE, which are step 1, step 8, and step 16, respectively. It can be observed that the magnitude of the noise is very large, and the power change reaches half of the extinction ratio of the FBGs. Even though the noise obliterates the original features of the FBG spectrum, a clean spectrum is obtained after SDAE denoising. As shown in Figure 3b, all the FBG spectra show smooth curves after SDAE denoising; even though the extinction ratio of the FBGs is changed after denoising, it does not affect the wavelength demodulation of the machine learning. The analysis of the signal-to-noise ratio (SNR) in Figure 4 corresponds to the spectrum depicted in Figure 3b. Figure 4a illustrates the SNR outcome without utilizing SDAE, while Figure 4b showcases the results following denoising with SDAE. The average SNR result without SDAE is 10.27 dB, whereas the average SNR result after SDAE denoising is 32.08 dB. This demonstrates an improvement in SNR of approximately 22 dB through the use of SDAE. It is important to note that this 22 dB improvement reflects the difference in SNR between the noisy and denoised spectra, rather than a fixed improvement solely attributed to SDAE.

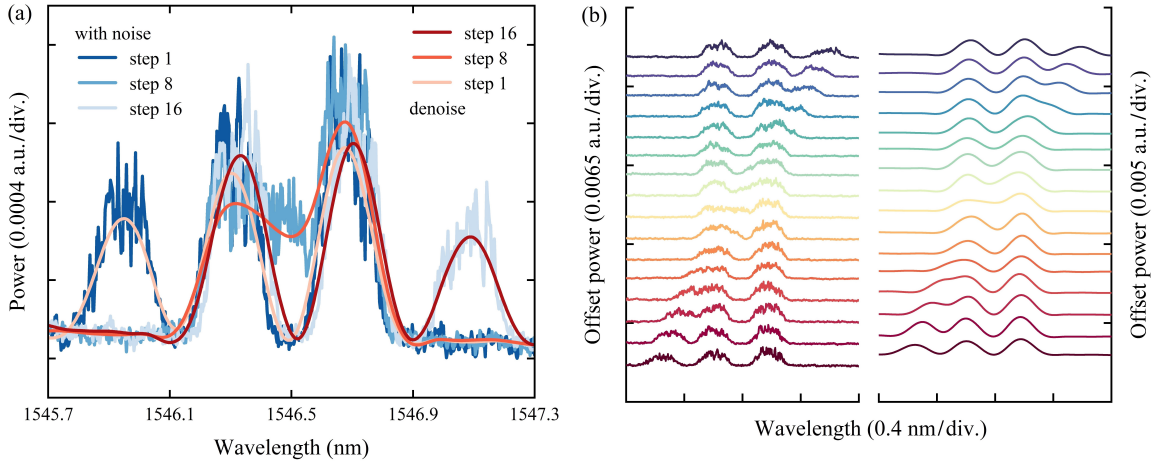

Figure 3. (**a**) Comparison of some FBG spectra before and after denoising; (**b**) Presentation of all FBG spectra (step 1 to step 16 in order) before and after denoising.

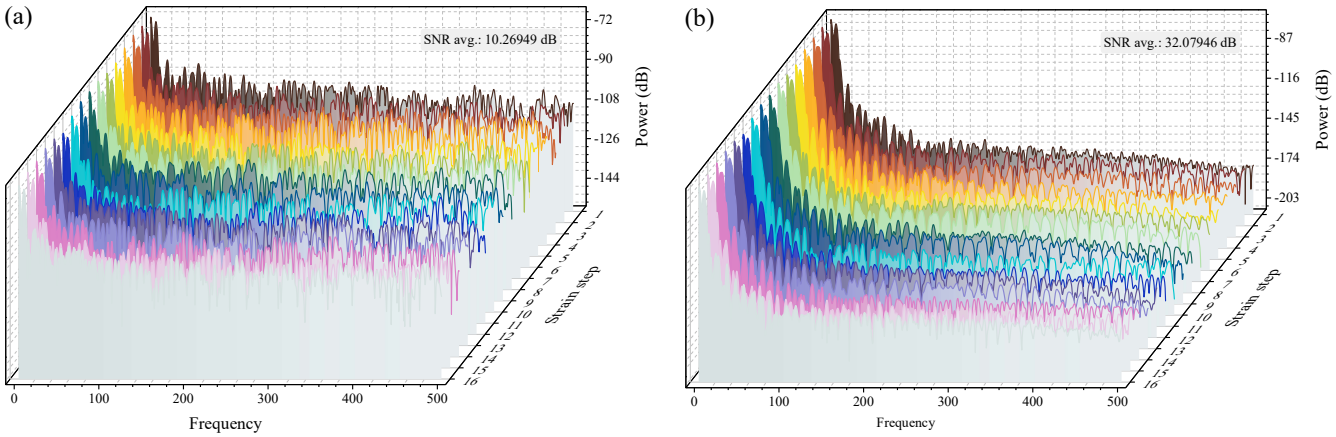

Figure 4. Signal-to-noise ratio analysis (**a**) before SDAE denoising; (**b**) after SDAE denoising.

Furthermore, as mentioned above, the ambient turbulence of the FSO can cause the peak power of the FBGs to be disturbed over time in addition to the noise. Figure 5 shows the power corresponding to each FBG peak after 19 spectral denoising for each of the three train steps 1, 8, and 16. The peak wavelength positions of the FBGs are set according to Figure 2. In previous studies, the peak powers of FBGs collected from repeated data with the same FBG position are mostly similar, and the differences, if any, are linear. However, in the FSO link used in this work, due to the turbulence floating, each FBG's peak power varies independently and randomly, which means that the peak spectra of FBGs are presented in a nonlinear manner. Therefore, the demodulation of non-linear peak power FBG spectra is also verified by machine learning for the first time.

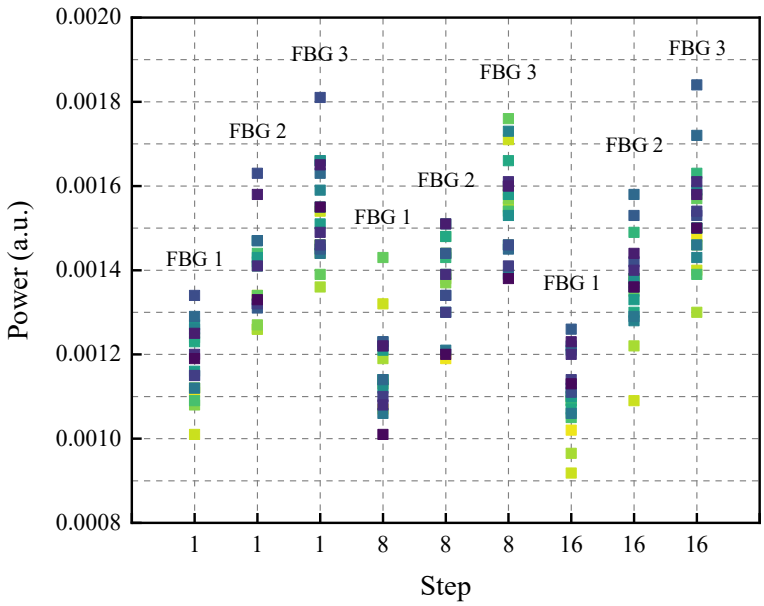

Figure 5. The peak power of FBGs for each of the 19 spectra collected under strain steps 1, 8, and 16.

4. DBN for Peak Wavelength Prediction

A DBN is a type of generative model that comprises a series of pre-trained layers of restricted Boltzmann machines (RBMs) [27–32]. This hierarchical arrangement enables DBNs to progressively acquire an abstract representation of the input data as it traverses through the layers. The training process for DBNs typically involves two primary phases: pre-training and fine-tuning. During the pre-training phase, each RBM captures the statistical properties of the input data and gradually learns deeper and more abstract features linked to the peak wavelength information. This approach enables the DBN to effectively

model the intricate relationships among signals from various FBG sensors, particularly when dealing with overlapping spectra. Once all layers have been pre-trained, the complete DBN can undergo fine-tuning using supervised learning methods, provided labeled data are available. This fine-tuning process entails adding the final output layer and utilizing backpropagation to adjust the network weights to minimize prediction errors. In the concluding stage of fine-tuning, the entire DBN is tuned through backpropagation to optimize the detection of peak wavelengths.

Figure 6 illustrates the main flow chart for the demodulation of the FBG spectrum with noise using DBN. After the FBG spectrum collection and SDAE denoising process, the data are also processed, labeled, and normalized for DBN model training. During DBN training, various parameters such as epoch number, batch size, hidden layer, hidden cell, and optimizer and activation functions need to be adjusted to achieve the optimal value of the detected peak wavelength. After the training process, it is confirmed whether the peak wavelength has converged or not, and if not, the parameters of the model are further modified. If the convergence is confirmed, the DBN model is used for wavelength prediction, and if the result is unsatisfactory, the stage of modifying various parameters of the model is reversed. If the result of the DBN model is satisfactory, then test data (20% of the total data) can be used to verify the effectiveness of the DBN model in predicting the wavelength. Various parameters of the adopted SDAE and DBN models are shown in Figure 7. Incidentally, the Adam optimizer is preferred in deep learning because of its computing efficiency and flexible learning rate capabilities. Faster and more dependable convergence is made possible by Adam's adjustment of learning rates for each parameter based on the first and second moments of gradients, in contrast to classical stochastic gradient descent (SGD), particularly in situations involving sparse gradients or noisy data [33]. Especially, according to the results of the previous study [21], the accuracy of the Adam optimizer is better than that of other optimizers, which is why this scheme adopts the Adam optimizer.

The final optimized DBN model is executed with 3 hidden layers, 32 batch sizes, and 200 epochs. These settings introduce non-linearity and enhance the network's ability to model complex relationships in the data. Figure 8 illustrates the training performance of the DBN in terms of training and validation loss and training and validation accuracy using these optimal parameters. The training loss decreases rapidly and stabilizes around zero at 200 epochs, reflecting effective learning of the training data. Similarly, the validation loss drops significantly early on and then stabilizes, indicating good generalization to unseen data without overfitting. By epoch 200, the training accuracy is close to 95% and the validation accuracy is close to 100%, albeit with some variance. Overall, DBN shows strong performance in learning and generalizing from data efficiently with high accuracy and low loss metrics.

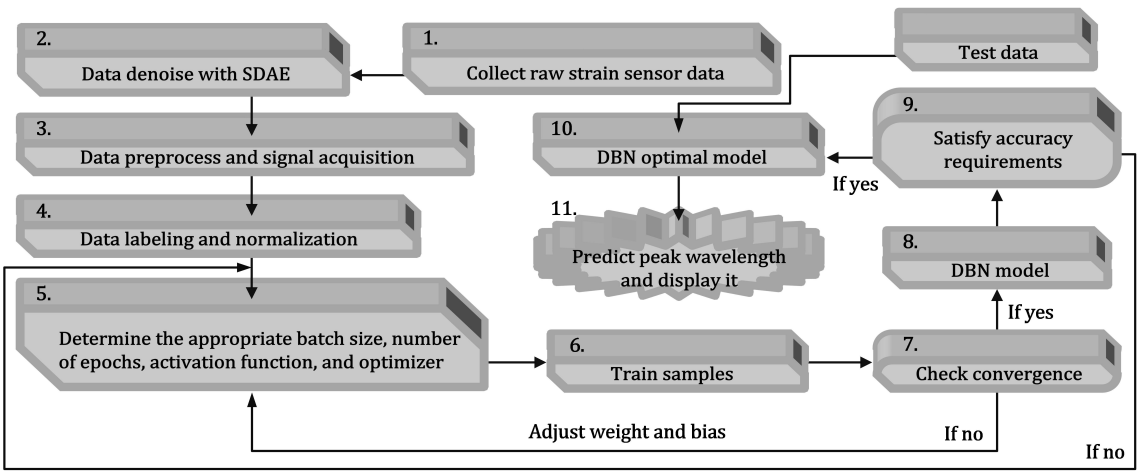

Figure 6. Flowchart of wavelength demodulation by DBN.

SDAE Encoder and Decoder

Parameter	Value
Hidden layer	4
Batch size	64
Epoch	300
Activation	Relu
Optimizer	Adam
Input dimension	304
Regularization	L2 (0.00001)
Dropout (Encoder)	0.3
Dropout (Decoder)	0
Neuron per layer (Encoder)	512, 256, 128, 64
Neuron per layer (Decoder)	128, 256, 512, 304

DBN Optimal Model

Parameter	Value
Hidden layer	3
Batch size	32
Epoch	200
Activation	Relu
Optimizer	Adam
Input shape	2001
Output shape	3
Neuron per layer	500

Figure 7. Parameters of the proposed SDAE and DBN models.

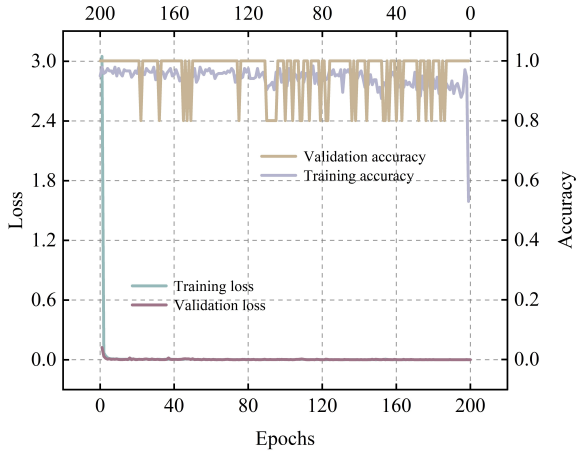

Figure 8. Training efficiency of the DBN model in terms of accuracy and loss.

Figure 9 shows the comparison of the wavelength prediction performance of different machine learning models in FBG spectra, in which the actual wavelength value of FBG and the predicted wavelength value of FBG can be used as parameters to substitute into the mean squared error (MSE), mean absolute error (MAE), and root mean square errors (RMSE) loss function to evaluate the performance. Gated Recurrent Unit (GRU) and Multi-Layer Perceptron (MLP) are very common machine learning models, which are used here to compare their performance with the DBN model for FBG wavelength prediction. DBNs are designed to learn hierarchical data representations through multiple layers of random latent variables, which enables them to capture complex and abstract features. Therefore, DBNs are particularly adept at complex signal demodulation compared to MLPs, which usually rely on more linear feature extraction methods and have difficulty capturing non-linear relationships. While GRUs are effective in handling time dependence in continuous data, they may not be able to adequately handle nonlinear spectral variations in FBG signals. DBN's multi-layer architecture combined with the robust reconstruction capability of SDAE enhances the model's ability to detect and remove noise at different scales. In addition, DBN usually requires fewer parameters to achieve comparable or even better performance, which reduces the risk of overfitting, especially when the training data is limited. Therefore, from the results, it can be seen that DBN gives the best results after the demodulation of the SDAE-denoised FBG spectrum by DBN, GRU, and MLP, no matter in terms of MSE, MAE, or RMSE. The performance of DBN with SDAE is expected to be better than without SDAE in terms of MSE, MAE, and RMSE metrics by 0.00277, 0.02353, and 0.02645, respectively. Hence, from the results, it can be seen that DBN gives the best results after the demodulation of SDAE-denoised FBG spectrum by DBN, GRU, and MLP, no matter in terms of MSE, MAE, or RMSE. The performance of DBN with SDAE is expected to be better than without SDAE. In comparison with the previous FBG demodulation work [21], the MSE, MAE, and RMSE obtained in this work are 0.00153, 0.019, and 0.0391,

respectively, which are close to the MSE, MAE, and RMSE obtained in the previous work, which are 0.0012, 0.015, and 0.0187, respectively, under the same use of DBN. Because of the similarity of the model setup and spectral sampling, the comparison is justified. Furthermore, the methodology employed in this study induces a non-linear variation in the individual FBG peak power over time for each sample, as opposed to consistent sampling in the previous work. This variation contributes to a slightly inferior demodulation of the FBG wavelengths compared with the previous study.

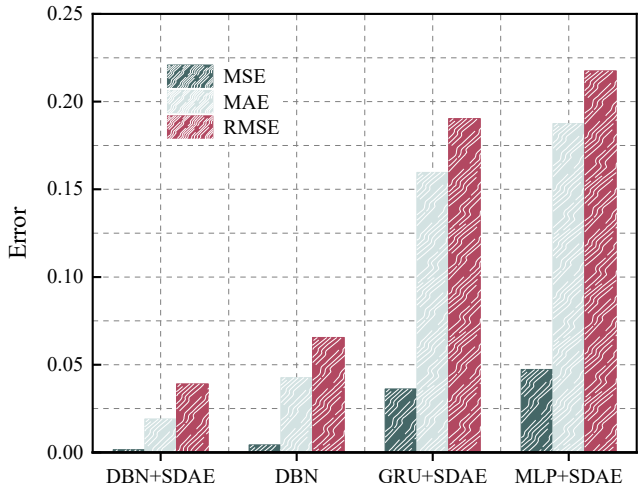

Figure 9. Performance comparison with different machine learning models.

Figure 10 illustrates the comparison between the actual FBG wavelength and the predicted FBG wavelength with 44 random selecting strain step points. Figure 10a shows the predicted wavelengths with SDEA denoising and then demodulated by DBN, while Figure 10b shows the predicted wavelengths without SDEA denoising and directly demodulated by DBN. It is obvious that the wavelength prediction results of FBG 1, FBG 2, and FBG 3 are better after SDEA denoising and then demodulation by DBN, regardless of whether the FBG spectra are overlapped or not. Incidentally, the resolution of OSA may limit the resolution of FBG wavelength demodulation to an upper limit of 0.02 nm [34], while the resolution of the smallest FBG wavelength demodulation in this work is 0.06 nm. Theoretically, the resolution of FBG wavelength demodulation using machine learning can be as high as 0.02 nm, but the present work focuses on FBG wavelength demodulation based on the denoising of noise caused by FSO rather than on resolution refinement.

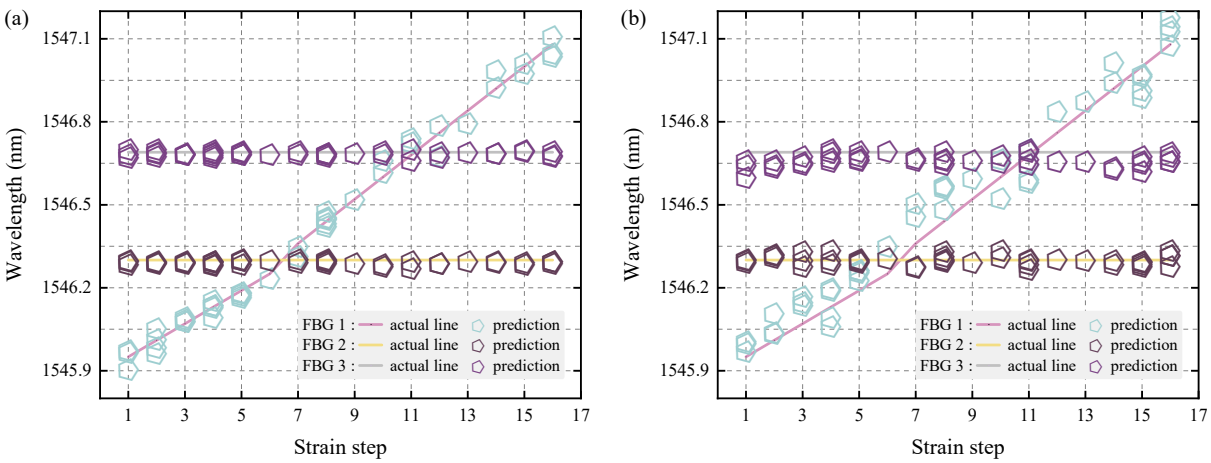

Figure 10. (**a**) FBG peak wavelength prediction after applying SDAE and DBN models. (**b**) FBG peak wavelength prediction after applying the DBN model only.

5. Conclusions

This study represents pioneering validation of the FBG sensing architecture based on FSO transmission, accounting for the non-linear peak power variation and spectral incidental noise arising from optical turbulence and airborne particle scattering. Additionally, it demonstrates the application of machine learning for the demodulation of FBG sensing wavelengths within this architecture. These results have encouraging ramifications for FBG sensing architectures that use FSO transmission in turbulent environments. Utilizing a sophisticated deep learning denoising method (the SDAE), noise in the FBG sensing spectrum is effectively reduced regardless of the wavelength and peak power distribution. Then, the FBG peak power attached to each data is inconsistent, and even in overlapping situations, the denoised FBG sensed spectrum can be demodulated by applying the DBN technique to precisely identify the sensed wavelengths of FBGs. The FBG wavelength demodulation results of the latter case are better than the former case by 0.00277, 0.02353, and 0.02645 in terms of MSE, MAE, and RMSE metrics when DBN is used alone versus when SDAE is used first and then DBN is used. As a result, the combined application of SDAE and DBN shows great promise for demodulating FBG spectra tainted by turbulence in the surrounding environment within the FSO architecture, thereby improving sensing accuracy and performance.

Author Contributions: Conceptualization, S.D.B., C.-K.Y., Y.C.M. and P.-C.P.; methodology, S.D.B., C.-K.Y. and Y.C.M.; software, S.D.B., Y.C.M., M.A.T. and A.M.D.; data curation, C.-K.Y., W.-L.L. and Z.-G.Z.; validation, S.D.B., C.-K.Y., M.A.T. and Y.C.M.; formal analysis, S.D.B., C.-K.Y. and A.M.D.; investigation, S.D.B., C.-K.Y., Y.C.M., A.M.D., M.A.T. and P.-C.P.; visualization, C.-K.Y.; writing—original draft preparation: C.-K.Y., S.D.B. and Y.C.M.; writing—review and editing: C.-K.Y.; supervision, P.-C.P. All authors have read and agreed to the published version of the manuscript.

Funding: This work was supported by the National Science and Technology Council, Taiwan, under Grant NSTC 112-2221-E-027-076-MY2.

Data Availability Statement: The data presented in this study are available in this article.

Conflicts of Interest: The authors declare no conflicts of interest.

References

1. Alias, M.A.; Ahmad, H.; Zaini, M.K.A.; Samion, M.Z.; Sa'ad, M.S.M.; Sing, L.K.; Grattan, K.T.V.; Rahman, B.M.A.; Brambilla, G.; Reduan, S.A.; et al. Optical Fiber Bragg Grating (FBG)-Based Strain Sensor Embedded in Different 3D-Printed Materials: A Comparison of Performance. *Measurement* **2024**, *225*, 114060. [CrossRef]
2. Schena, E.; Tosi, D.; Saccomandi, P.; Lewis, E.; Kim, T. Fiber Optic Sensors for Temperature Monitoring During Thermal Treatments: An Overview. *Sensors* **2016**, *16*, 1144. [CrossRef]
3. Morais, E.; Pontes, M.J.; Marques, C.; Leal-Junior, A. Liquid level sensor with two FBGs embedded in a PDMS diaphragm: Analysis of the linearity and sensitivity. *Sensors* **2022**, *22*, 1268. [CrossRef] [PubMed]
4. Burhanuddin, W.A.F.W.; Ahmad, H.; Alias, M.A.; Sa'ad, M.S.M.; Sun, S.; Ismail, M.F. Multi-Parameter Fiber Bragg Grating (FBG)-based Sensor Fabricated using 3D Printing Technology for Precise Measurement of Vertical Earth and Pore Pressure. *IEEE Sens. J.* **2024**, *24*, 25793–25801. [CrossRef]
5. Avellar, L.; Marques, C.A.; Caucheteur, C.; Frizera, A. Comprehensive Evaluation of Tilted Fiber Bragg Grating (TFBG) Sensors for Characterizing Oil-Water Emulsions: A Study on the Impact of Surfactant Concentration and Mixing Speed. *IEEE Sens. J.* **2024**, *24*, 7824–7831. [CrossRef]
6. Nascimento, M.; Inácio, P.; Paixão, T.; Camacho, E.; Novais, S.; Santos, T.G.; Fernandes, F.M.B.; Pinto, J.L. Embedded fiber sensors to monitor temperature and strain of polymeric parts fabricated by additive manufacturing and reinforced with NiTi wires. *Sensors* **2020**, *20*, 1122. [CrossRef]
7. Macedo, L.; Souza, E.A.; Frizera, A.; Pontes, M.J.; Marques, C.; Leal-Junior, A. Static and Dynamic Multiparameter Assessment of Structural Elements using Chirped Fiber Bragg Gratings. *Sensors* **2023**, *23*, 1860. [CrossRef]
8. Kanwal, F.; Atieh, A.; Ghafoor, S.; Haq, A.U.; Qureshi, K.K.; Aziz, I.; Mirza, J. Remote Monitoring of Sleep Disorder Using FBG Sensors and FSO Transmission System Enabled Smart Vest. *Eng. Res. Express* **2024**, *6*, 025337. [CrossRef]
9. Yu, Y.L.; Liaw, S.K.; Chou, H.H.; Le-Minh, H.; Ghassemlooy, Z. A Hybrid Optical Fiber and FSO System for Bidirectional Communications Used in Bridges. *IEEE Photonics J.* **2015**, *7*, 1–9. [CrossRef]
10. Correia, V.D.; Fernandes, M.A.; Monteiro, P.P.; Guiomar, F.P.; Fernandes, G.M. On the Impact and Mitigation of Turbulence in Fiber-Coupled FSO Systems. *IEEE Access* **2024**, *12*, 69505–69516. [CrossRef]

11. Kazaura, K.; Omae, K.; Suzuki, T.; Matsumoto, M.; Mutafungwa, E.; Korhonen, T.O.; Murakami, T.; Takahashi, K.; Matsumoto, H.; Wakamori, K.; et al. Enhancing Performance of Next Generation FSO Communication Systems Using Soft Computing Based Predictions. *Opt. Express* **2006**, *14*, 4958–4968. [CrossRef]
12. Fernandes, M.A.; Fernandes, G.M.; Brandão, B.T.; Freitas, M.M.; Kaai, N.; Tomeeva, A.; Wielen, B.V.D.; Reid, J.; Raiteri, D.; Monteiro, P.P.; et al. 4 Tbps+ FSO Field Trial Over 1.8 km with Turbulence Mitigation and FEC Optimization. *J. Light. Technol.* **2024**, *42*, 4060–4067. [CrossRef]
13. Manie, Y.C.; Li, J.-W.; Peng, P.-C.; Shiu, R.-K.; Chen, Y.-Y.; Hsu, Y.-T. Using a Machine Learning Algorithm Integrated with Data De-Noising Techniques to Optimize the Multipoint Sensor Network. *Sensors* **2020**, *20*, 1070. [CrossRef]
14. Rudloff, G.; Soto, M.A. Multi-Peak Wavelength Detection of Spectrally-Overlapped Fiber Bragg Grating Sensors Through a CNN-Based Autoencoder. *IEEE Sens. J.* **2024**, *24*, 20674–20687. [CrossRef]
15. Jiang, H.; Tang, R.; Wang, C.; Zhao, Y.; Li, H. Recognition and Localization of FBG Temperature Sensing Based on Combined CDAE and 1-DCNN. *IEEE Sens. J.* **2024**, *24*, 10125–10137. [CrossRef]
16. Sun, Y.; Di, K.; Deng, Y.; Hu, J. Demodulation of Different Quantities of Overlapping Spectra in FBG Sensors Based on Combined Conv-TasNet and LSTM. *IEEE Sens. J.* **2024**, *24*, 28860–28868. [CrossRef]
17. Cibira, G.; Glesk, I.; Dubovan, J. SNR-Based Denoising Dynamic Statistical Threshold Detection of FBG Spectral Peaks. *J. Light. Technol.* **2022**, *41*, 2526–2539. [CrossRef]
18. Shan, L.; Yu, M.; Xia, J.; Xin, J.; Deng, C.; Zhu, L. Overlapped Spectral Demodulation of Fiber Bragg Grating Using Convolutional Time-Domain Audio Separation Network. *Opt. Eng.* **2023**, *62*, 066104. [CrossRef]
19. Yao, C.-K.; Peng, C.-H.; Chen, H.-M.; Hsu, W.-Y.; Lin, T.-C.; Manie, Y.C.; Peng, P.-C. One Raman DTS Interrogator Channel Supports a Dual Separate Path to Realize Spatial Duplexing. *Sensors* **2024**, *24*, 5277. [CrossRef]
20. Lionis, A.; Sklavounos, A.; Stassinakis, A.; Cohn, K.; Tsigopoulos, A.; Peppas, K.; Aidinis, K.; Nistazakis, H. Experimental machine learning approach for optical turbulence and FSO outage performance modeling. *Electronics* **2023**, *12*, 506. [CrossRef]
21. Bogale, S.D.; Yao, C.-K.; Manie, Y.C.; Zhong, Z.-G.; Peng, P.-C. Wavelength-Dependent Bragg Grating Sensors Cascade an Interferometer Sensor to Enhance Sensing Capacity and Diversification through the Deep Belief Network. *Appl. Sci.* **2024**, *14*, 7333. [CrossRef]
22. Tefera, M.A.; Dehnaw, A.M.; Manie, Y.C.; Yao, C.-K.; Bogale, S.D.; Peng, P.-C. Advanced Denoising and Meta-Learning Techniques for Enhancing Smart Health Monitoring Using Wearable Sensors. *Future Internet* **2024**, *16*, 280. [CrossRef]
23. Xing, C.; Ma, L.; Yang, X. Stacked Denoise Autoencoder Based Feature Extraction and Classification for Hyperspectral Images. *J. Sens.* **2016**, *2016*, 3632943. [CrossRef]
24. Ouyang, Y.; Wang, H. Adaptive Denoising Combined Model with SDAE for Transient Stability Assessment. *Electr. Power Syst. Res.* **2023**, *214*, 108948. [CrossRef]
25. Vincent, P.; Larochelle, H.; Lajoie, I.; Bengio, Y.; Manzagol, P.A.; Bottou, L. Stacked Denoising Autoencoders: Learning Useful Representations in a Deep Network with a Local Denoising Criterion. *J. Mach. Learn. Res.* **2010**, *11*, 3371–3408.
26. Majumdar, A.K. Free-Space Laser Communication Performance in the Atmospheric Channel. *J. Opt. Fiber Commun. Rep.* **2005**, *2*, 345–396. [CrossRef]
27. Akbaş, A.; Buyrukoğlu, S. Deep Belief Network Based Wireless Sensor Network Connectivity Analysis. *Balk. J. Electr. Comput. Eng.* **2023**, *11*, 262–266. [CrossRef]
28. Sohn, I. Deep Belief Network Based Intrusion Detection Techniques: A Survey. *Expert Syst. Appl.* **2021**, *167*, 114170. [CrossRef]
29. Li, C.; Wang, Y.; Zhang, X.; Gao, H.; Yang, Y.; Wang, J. Deep Belief Network for Spectral–Spatial Classification of Hyperspectral Remote Sensor Data. *Sensors* **2019**, *19*, 204. [CrossRef]
30. Larochelle, H.; Bengio, Y.; Louradour, J.; Lamblin, P. Exploring Strategies for Training Deep Neural Networks. *J. Mach. Learn. Res.* **2009**, *10*, 1–40.
31. Kale, A.P.; Wahul, R.M.; Patange, A.D.; Soman, R.; Ostachowicz, W. Development of Deep Belief Network for Tool Faults Recognition. *Sensors* **2023**, *23*, 1872. [CrossRef] [PubMed]
32. Hinton, G.E.; Osindero, S.; Teh, Y.W. A Fast Learning Algorithm for Deep Belief Nets. *Neural Comput.* **2006**, *18*, 1527–1554. [CrossRef] [PubMed]
33. Kingma, D.P. Adam: A Method for Stochastic Optimization. *arXiv* **2014**, arXiv:1412.6980.
34. Du, J.; He, Z. Sensitivity Enhanced Strain and Temperature Measurements based on FBG and Frequency Chirp Magnification. *Opt. Express* **2013**, *21*, 27111–27118. [CrossRef] [PubMed]